Proceedings of the International MultiConference of Engineers and Computer Scientists 2011 Vol II,
IMECS 2011, March 16 - 18, 2011, Hong Kong

A Design of Intelligent Actuator Logic using Fuzzy Control for EMB System

Kuktae Kim, Qing Li, Chanmin Park, Kyoil Hwang, Joogon Kim, and Hunmo Kim

***Abstract*—This paper focuses on the design of intelligent actuator logic for Electro-Mechanical Brake (EMB) system using fuzzy control. Previous studies simplified EMB system as a linear system or removed coulomb friction and backlash for the convenience of calculation. However, nonlinear components such as coulomb friction and backlash should be considered because the inherent nonlinearity in the high operating speed of EMB system is critical. Therefore, in this paper, we adopt full Brake by Wire (BBW) model of EMB system. Unlike Electro-Hydraulic Brake (EHB) system, EMB has no hydraulic back-up system, and is operated totally by electric and electro-mechanical components. Therefore, safety is the one of the most important problems in designing an EMB system. To control the EMB system, we developed fuzzy logic controller, which is effective in a complex and nonlinear system. MATLAB SIMULINK is used to provide the verification of the control performance. Simulation results show that the proposed fuzzy logic controller forces the EMB actuator to follow the command input precisely. This study will be a base of further research, whose purpose is to develop an intelligent actuator logic using adaptive fuzzy control for EMB system in noise and disturbance.**

***Index Terms*—X-by-Wire, EMB system, fuzzy algorithm, nonlinear control, intelligent brake actuator logic**

I. Introduction

The automotive industry has developed X-by-Wire system, which replaces vehicles' hydraulic systems with wires, micro controllers, and electric machines, not only to increase vehicle safety and performance but also to reduce manufacturing costs and weight. Brake-by-Wire (BBW), the one of X-by-Wire systems, has been actively studied [1]–[7]. BBW means the brake pedal and the brake actuators are connected by wire without any hydraulic or mechanical connection. In this paper, we focus on the design of intelligent actuator logic using fuzzy control for Electro-Mechanical Brake (EMB) system. EMB systems have some benefits such as assistant function (ABS, TCS, ESP, etc), weight reduction, environmentally friend, manufacturing costs reduction, and maintenance costs reduction. The EMB system requires more precise control than a conventional brake system because EMB system does not have any hydraulic or mechanical connection between brake pedal and brake actuator. Previous studies of the BBW system have lacked detailed mathematic modeling, and simplified system into linear or reduced nonlinear part such as coulomb friction and backlash for the convenience of calculation [3]. In this paper, we adopt full EMB modeling because nonlinear components are critical in the high speed operating system. Joogon Kim *et al*. proposed PI control for the EMB actuator control [3]. Simplifying model and PI control allow people to perform quick calculation and conveniently use conventional tools. However, simplifying model is not accurate in high speed. Wenzhe Lu proposed backstepping control of switched reluctance machines for EMB [4]. However, backstepping control demands precise parameter values. Jaeho Kwak proposed advanced nonlinear Indirect Adaptive Robust Control (IARC) [2]. However, ARC copes with the system, whose parameters being controlled are slowly time-varying or uncertain. In this paper, we propose fuzzy logic control as intelligent actuator logic for EMB system because fuzzy logic is effective in a complex and nonlinear system. This study is a ground work for next research to develop an intelligent actuator logic using adaptive fuzzy control for EMB system, which is effective in noise and disturbance. Adaptive fuzzy control changes the fuzzy rule based on the environmental condition, so it can be used even for an unpredictable situation and for situations with parameters which affect the input variables.

The rest of this paper is organized as follows: Complete EMB model is developed in Section II. Simulation results for the complete nonlinear model and the validity of model are also represented in the Section. Section III represents fuzzy control logic for EMB actuator. Simulation results of fuzzy logic control logic to verify the performance of the controller is represented in Section IV. Lastly, Section V shows conclusion and future work.

II. Complete EMB Model Development

Fig. 1 shows the sectional drawing of EMB [1], [2]. We referred [1], [2] to develop full modeling of EMB system. A rigorous modeling of complete BBW system, without any reduction or simplification, enables us to satisfy the simulation

Manuscript received December 07, 2010; revised January 20, 2011. This work was supported by the Ministry of Knowledge Economy.

K. T. Kim is with Mechanical Engineering Department, Sungkyunkwan University, Suwon, Gyonggi-do, 440-746, Korea (e-mail: from82@skku.edu).

Qing Li is with Mechanical Engineering Department, Sungkyunkwan University, Suwon, Gyonggi-do, 440-746, Korea (e-mail: liqing1120@gmail.com).

C. M. Park is with Mechanical Engineering Department, Sungkyunkwan University, Suwon, Gyonggi-do, 440-746, Korea (e-mail: thecall84@gmail.com).

K. I. Hwang is with Mechanical Engineering Department, Sungkyunkwan University, Suwon, Gyonggi-do, 440-746, Korea (e-mail: hki0114@naver.com).

J. G. Kim was with Central R&D Center, Mando Corporation, 413-5, Gomae-dong, Giheung-gu, Yongin-si, Gyeonggi-do, 446-901, Korea (e-mail: djgkim@mando.com).

H. M. Kim is with Mechanical Engineering Department, Sungkyunkwan University, Suwon, Gyong-gi, 440-746, Korea (phone: 82-31-290-7450; fax: 82-31-290-7666; e-mail: kimhm@me.skku.ac.kr)

ISBN: 978-988-19251-2-1
ISSN: 2078-0958 (Print); ISSN: 2078-0966 (Online)

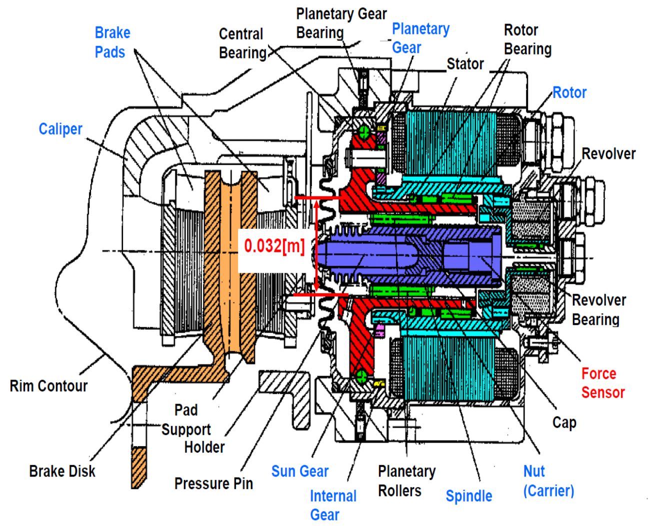

Fig. 1. Sectional drawing of the EMB

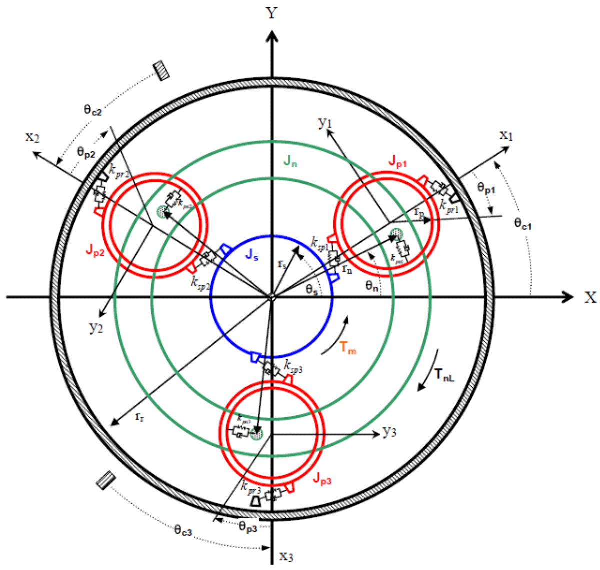

Fig. 2. PGT Medel for Rotational Dynamics

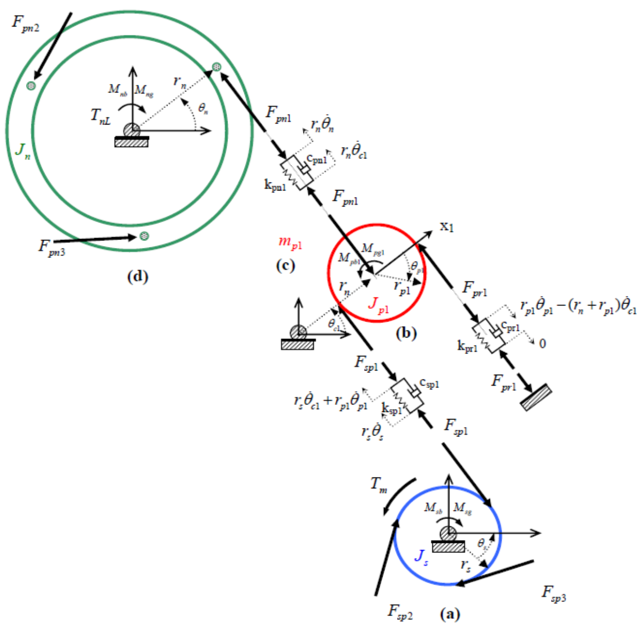

Fig. 3. Dynamic models of (a) a sun gear (motor rotor), (b) a planetary gear (rotation) (c) a planetary gear (revolution), and (d) a nut carrier

TABLE I
NOTATIONS USED IN FIG. 2 AND FIG. 3

Symbol	Meaning
r_s [m]	Pitch radius of sun gear
r_{pi} [m]	Pitch radius of planetary gear i
r_r [m]	Pitch radius of ring gear
r_n [m]	Radius of nut carrier thrusting the spindle
θ_s [rad]	Absolute angular displacement of sun gear in the world frame XY plane
θ_{pi} [rad]	Relative angular displacement of planetary gear i in the moving coordinate x_iy_i
θ_{ci} [rad]	Absolute angular displacement of center of planetary gear i in XY plane
θ_n [rad]	Absolute angular displacement of nut carrier pin in XY plane
J_s [kgm^2]	Inertia moment of sun gear with respect to the center
J_{pi} [kgm^2]	Inertia moment of planetary gear I with respect to its center
m_{pi} [kg]	Mass of planetary gear i
J_n [kgm^2]	Inertia moment of nut carrier
c_{spi} [Ns/m]	Mesh damping between sun gear and planetary gear i
c_{pri} [Ns/m]	Mesh damping between planetary gear and ring gear i
c_{pni} [Ns/m]	Mesh damping between planetary gear and nut carrier pin i
k_{spi} [N/m]	Mesh stiffness between sun gear and planetary gear i
k_{pri} [N/m]	Mesh stiffness between planetary gear and ring gear i
k_{pni} [N/m]	Bearing stiffness between planetary gear and nut carrier i
M_{sb} [Nm]	Bearing friction moment of sun gear
M_{sg} [Nm]	Gear friction moment of sun gear
M_{pbi} [Nm]	Bearing friction moment of nut carrier
M_{pgi} [Nm]	Gear friction moment of planetary gear i
M_{nb} [Nm]	Bearing friction moment of nut carrier
M_{ng} [Nm]	Screw friction moment of nut carrier
T_m [Nm]	Motor torque
T_{nL} [Nm]	Torque load of nut carrier to thrust the spindle
F_{spi} [N]	Transmission force between sun gear and planetary gear i
F_{pri} [N]	Transmission force between planetary gear and ring gear i
F_{pni} [N]	Transmission force between planetary gear and nut carrier pin i

results because it is highly similar to the real model and it is effective to apply the simulation result to the real EMB system later. The single state Planetary Gear Train (PGT) is considered as the EMB in this paper. Fig. 2 represents the PGT, which consists of a sun gear connected with motor rotor, an internal ring gear fixed with caliper housing, and 3 identical planetary gears coupling the sun gear with the internal ring gear [1], [2]. Fig. 4 illustrates a free body diagram for a pair of power transmission elements for planetary gear i=1. The notations used in Fig. 2 and Fig. 3 are represented in the Table I [2].

Using Lagrange's method, we can find the equations of the motion for PGT [1], [2]. The equations of the sun Gear (motor rotor) can be represented such as (1) to (3) [1], [2]:

$$J_s\ddot{\theta}_s + C_s\dot{\theta}_s + C_{sn}(\dot{\theta}_s - \dot{\theta}_n) + \mathrm{sgn}(\dot{\theta}_s)[M_{s0} + M_{sg1}(r_sk_{sp}|f_{sp1}| + r_sc_{sp}|f_{sp2}|)] + r_sk_{sp}f_{sp1} + r_sc_{sp}f_{sp2} = T_m \quad (1)$$

ISBN: 978-988-19251-2-1
ISSN: 2078-0958 (Print); ISSN: 2078-0966 (Online)

$$f_{sp1} = \begin{cases} 0 & for \quad (r_s\theta_s - r_s\theta_c - r_p\theta_p) < \left|B_{sp}\right| \\ (r_s\theta_s - r_s\theta_c - r_p\theta_p - B_{sp}) & for \quad (r_s\theta_s - r_s\theta_c - r_p\theta_p) \ge B_{sp} \\ (r_s\theta_s - r_s\theta_c - r_p\theta_p + B_{sp}) & for \quad (r_s\theta_s - r_s\theta_c - r_p\theta_p) \le -B_{sp} \end{cases} \quad (2)$$

$$f_{sp2} = \begin{cases} 0 & for \quad (r_s\theta_s - r_s\theta_c - r_p\theta_p) < \left|B_{sp}\right| \\ r_s\dot{\theta}_s - r_s\dot{\theta}_c - r_p\dot{\theta}_p & for \quad (r_s\theta_s - r_s\theta_c - r_p\theta_p) \ge \left|B_{sp}\right| \end{cases}, \quad (3)$$

where C_s is viscous friction coefficient depending on rotor speed, C_{sn} is viscous friction coefficient depending on relative speed between rotor and nut carrier, M_{sb0} is static friction moment of rotor bearing, and M_{sg0} is static friction moment of gear contacting. M_{sg1} is gear friction coefficient depending on transmission load, $M_{s0} = M_{sb0} + M_{sg0}$, the lumped mesh stiffness is $k_{sp} = \sum_{i=1}^{3} k_{spi}$, and the lumped damping is $c_{sp} = \sum_{i=1}^{3} c_{spi}$.

The equations of the planetary gear rotation are represented such as (4) to (6) [1], [2]:

$$J_p(\ddot{\theta}_p - \ddot{\theta}_s) + C_p\dot{\theta}_p + \mathrm{sgn}(\dot{\theta}_p)[M_{p0} + M_{pg1}(r_pk_{pr}\left|f_{pr1}\right| + r_pc_{pr}\left|f_{pr2}\right|)] + r_pk_{pr}f_{pr1} + r_pc_{pr}f_{pr2} - r_pk_{sp}f_{sp1} - r_pc_{sp}f_{sp2} = 0 \quad (4)$$

$$f_{pr1} = \begin{cases} 0 & for \quad \left|(r_p\theta_p - (r_n + r_p)\theta_c)\right| < B_{pr} \\ (r_p\theta_p - (r_n + r_p)\theta_c - B_{pr}) & for \quad (r_p\theta_p - (r_n + r_p)\theta_c) \ge B_{pr} \\ (r_p\theta_p - (r_n + r_p)\theta_c + B_{pr}) & for \quad (r_p\theta_p - (r_n + r_p)\theta_c) \le -B_{pr} \end{cases} \quad (5)$$

$$f_{pr2} = \begin{cases} 0 & for \quad \left|r_p\theta_p - (r_n + r_p)\theta_c\right| < B_{pr} \\ (r_p\dot{\theta}_p - (r_n + r_p)\dot{\theta}_c) & for \quad \left|r_p\theta_p - (r_n + r_p)\theta_c\right| \ge B_{pr} \end{cases}, \quad (6)$$

where the planetary gear radius is $r_p = r_{pi}(i = 1-3)$, the rotational displacement of a planetary is $\theta_p = \theta_{pi}(i = 1-3)$, and the revolutional displacement of a planetary gear is $\theta_c = \theta_{ci}$. The lumped planetary inertia is $J_p = \sum_{i=1}^{3} J_{pi}$, as well as the lumped mesh stiffness and damping are $k_{pr} = \sum_{i=1}^{3} k_{pri}$, and $c_{pr} = \sum_{i=1}^{3} c_{pri}$. The lumped viscous damping is $C_p = \sum_{i=1}^{3} C_{pi}$, where C_{pi} is the viscous friction coefficient depending on the rotational speed of planetary gear i. Also, the friction terms can be expressed as a lumped expression by $M_{p0} = \sum_{i=1}^{3} M_{p0i}$, where M_{p0i} is the static friction moment of bearing for planetary gear i, and $M_{pg1} = \sum_{i=1}^{3} M_{pg1i}$, where M_{pg1i} is the gear friction coefficient depending on transmission load for gear i. B_{pr} is the backlash clearance between the planetary gear and the fixed internal ring gear.

Equations (7) to (9) represent the equations of the planetary gear revolution [1], [2].

$$(J_p + m_pr_n^2)\ddot{\theta}_c - J_p\ddot{\theta}_p + r_nk_{pn}f_{pn1} + r_nc_{pn}f_{pn2} - C_p\dot{\theta}_p - \mathrm{sgn}(\dot{\theta}_p) [M_{p0} + M_{pg1}(r_pk_{pr}\left|f_{pr1}\right| + r_pc_{pr}\left|f_{pr2}\right|)] - r_sk_{sp}f_{sp1} - r_sc_{sp}f_{sp2} - (r_n + r_p)k_{pr}f_{pr1} - (r_n + r_p)c_{pr}f_{pr2} = 0 \quad (7)$$

$$f_{pn1} = \begin{cases} 0 & for \quad r_n\left|(\theta_c - \theta_n)\right| < B_{pn} \\ r_n(\theta_c - \theta_n) - B_{pn} & for \quad r_n(\theta_c - \theta_n) \ge B_{pn} \\ r_n(\theta_c - \theta_n) + B_{pn} & for \quad r_n(\theta_c - \theta_n) \le -B_{pn} \end{cases} \quad (8)$$

$$f_{pn2} = \begin{cases} 0 & for \quad r_n\left|(\theta_c - \theta_n)\right| < B_{pn} \\ r_n(\dot{\theta}_c - \dot{\theta}_n) & for \quad r_n\left|(\theta_c - \theta_n)\right| \ge B_{pn} \end{cases}, \quad (9)$$

where the lumped mass is $m_p = \sum_{i=1}^{3} m_{pi}$, the lumped contacting bearing stiffness is $k_{pn} = \sum_{i=1}^{3} k_{pni}$, and the lumped contacting bearing damping is $c_{pn} = \sum_{i=1}^{3} c_{pni}$. B_{pn} is the contacting bearing clearance between the planetary gear and the nut carrier pin.

Equations (10) to (12) show the equations of nut carrier as follows [1], [2]:

$$J_n\ddot{\theta}_n + C_n\dot{\theta}_n + C_{sn}(\dot{\theta}_n - \dot{\theta}_s) + \mathrm{sgn}(\dot{\theta}_n)[M_{n0} + M_{n1}(K_{ns}\left|f_{ns1}\right| + C_{ns}\left|f_{ns2}\right|)] + \left(\frac{p}{2\pi}\right)(K_{ns}f_{ns1} + C_{ns}f_{ns2}) - r_nk_{pn}f_{pn1} - r_nc_{pn}f_{pn2} = 0 \quad (10)$$

$$f_{ns1} = \begin{cases} 0 & for \quad \left|(\frac{p}{2\pi}\theta_n + z_b - z_s)\right| < B_{ns} \\ (\frac{p}{2\pi}\theta_n + z_b - z_s - B_{ns}) & for \quad (\frac{p}{2\pi}\theta_n + z_b - z_s) \ge B_{ns} \\ (\frac{p}{2\pi}\theta_n + z_b - z_s + B_{ns}) & for \quad (\frac{p}{2\pi}\theta_n + z_b - z_s) \le -B_{ns} \end{cases} \quad (11)$$

$$f_{ns2} = \begin{cases} 0 & for \quad \left|(\frac{p}{2\pi}\theta_n + z_b - z_s)\right| < B_{ns} \\ (\frac{p}{2\pi}\dot{\theta}_n + \dot{z}_b - \dot{z}_s) & for \quad \left|(\frac{p}{2\pi}\theta_n + z_b - z_s)\right| \ge B_{ns} \end{cases}, \quad (12)$$

where C_n is is viscous damping coefficient depending on nut rotational speed, and C_{sn} is the viscous damping coefficient depending on relative rotation speed between the nut carrier and the motor rotor. $M_{n0} = M_{nb0} + M_{ng0}$, where M_{nb0} is the static friction moment, and M_{ng0} is the friction moment depending on the transmission load moment. $M_{n1} = M_{nb1}\left(r_n\frac{2\pi}{p}\right) + M_{ng1}$, K_{ns} is contacting stiffness between nut carrier and spindle, and C_{ns} is contacting damping between nut carrier and spindle. Also, p is the pitch of the roller screw, z_s is the spindle displacement, z_b is the brake caliper displacement, and B_{ns} is the backlash clearance between the nut carrier and the spindle.

The equations of spindle can be represented such as (13) to (15) [1], [2]:

$$m_{sp}\ddot{z}_s + C_{sb}(\dot{z}_s - \dot{z}_b) + K_{sp1}ff_{sp1} + C_{sp1}ff_{sp2} - K_{ns}f_{ns1} - C_{ns}f_{ns2} = 0 \quad (13)$$

ISBN: 978-988-19251-2-1
ISSN: 2078-0958 (Print); ISSN: 2078-0966 (Online)

$$ff_{sp1} = \begin{cases} 0 & for \quad z_s < BG \\ z_s - BG & for \quad z_s \geq BG \end{cases} \tag{14}$$

$$ff_{sp2} = \begin{cases} 0 & for \quad z_s < BG \\ \dot{z}_s & for \quad z_s \geq BG \end{cases}, \tag{15}$$

where C_{sb} is sliding damping between spindle and brake caliper, K_{sp1} is stiffness of the actuator side pad, C_{sp1} is damping of the actuator side pad, and BG is gap clearance between the actuator side pad and the disk rotor.

Equation (16) represents the equation of brake caliper [1], [2].

$$m_b \ddot{z}_b + C_{sb}(\dot{z}_b - \dot{z}_s) + K_c z_b + C_c \dot{z}_b - F_{bt} + K_{ns} f_{ns1} + C_{ns} f_{ns2} = 0, \tag{16}$$

where K_c is stiffness of brake caliper including the caliper side pad, C_c is damping of brake caliper, and F_{bt} is caliper frictional force coming from the sliding pin.

The simulation result of the equations for full model is represented in Fig. 4. We applied 20V as input voltage from initial time to 0.2 second, -20V from 0.2 second to 0.4 second, and 0V from 0.4 second to 0.6 second. Until around 0.08 second, the spindle position increase sharply and clamping force is 0N. This is because the EMB system is gapping mode, on which brake pad does not hit the brake disk, during the time. Clamping force increases dramatically and the spindle position increase slowly from 0.08 second to 0.2 second because the EMB system is clamping mode, where brake pad hits the brake disk. After 0.2 second, -20V is inputted as voltage input, then clamping force decreases sharply and the spindle position decreases slowly. After 0.28 seconds, the EMB system returns to gapping mode. Clamping force remains zero and spindle position starts to decrease rapidly. From 0.4 second, the voltage input is released. Clamping force stays zero and spindle position keeps about -0.25×10^{-4} m, which is the last position when voltage is removed. We can confirm the validation of the EMD full model equations and simulation result by comparing simulation result to [1], [2].

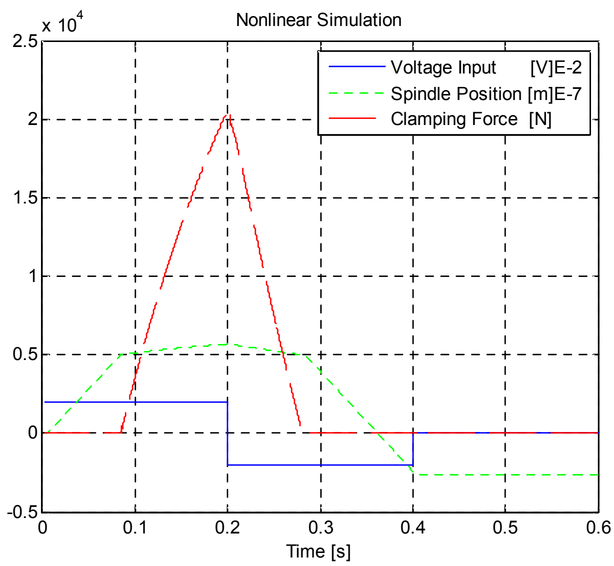

Fig. 4. Simulation result for Full model

III. FUZZY CONTROL

Fuzzy logic control has some benefits such as the expressible ability to simulate human being's fuzzy behaviors. It is effective at handling the uncertainties and nonlinearities associated with complex control systems. In this paper, input to the fuzzy controller is the error of clamping force, whereas the output is the voltage of the EMB actuator. The error of clamping force and voltage are fuzzified into seven fuzzy sets: negative big (NB), negative medium (NM), negative small (NS), zero (ZE), positive small (PS), positive medium (PM), positive big (PB). Fig. 5 represents fuzzy membership function of input value, the error of clamping force.

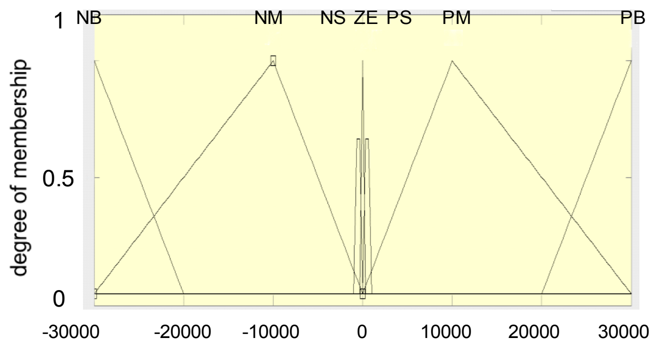

Fig. 5. Fuzzy membership function of input value

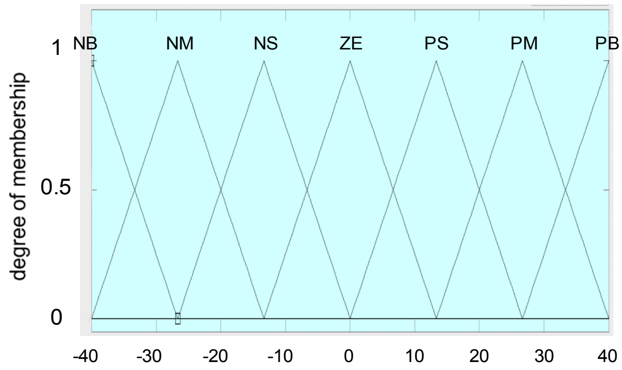

Fig. 6. Fuzzy membership function of output value

TABLE III
Rule base for fuzzy logic controller

	e						
	NB	NM	NS	Zero	PS	PM	PB
out	NB	NM	NS	Zero	PS	PM	PB

Fig. 6 shows fuzzy membership function of output value, voltage. Triangular shapes are chosen for the membership function. SIMULINK block for fuzzy logic control of complete EMB system is represented in Appendix. Rule base for fuzzy logic controller is shown in Table III.

IV. RESULTS

To check the performance of fuzzy logic controller, we produce the command input, and clamping force is generated by fuzzy logic controller to follow the command input. The results are shown from Fig. 7 to Fig. 9. Fuzzy logic controller allows actuator to follow command input precisely. There is a time delay between command input and actuator output from 0.1 second to 0.18 second. This is a gapping mode, noncontact

ISBN: 978-988-19251-2-1
ISSN: 2078-0958 (Print); ISSN: 2078-0966 (Online)

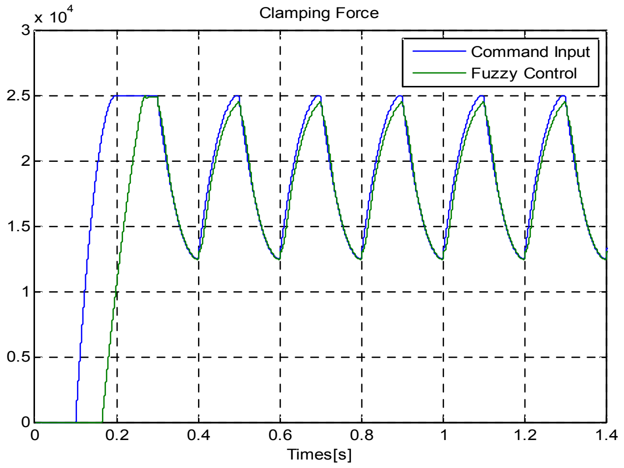

Fig. 7. Command input and clamping force

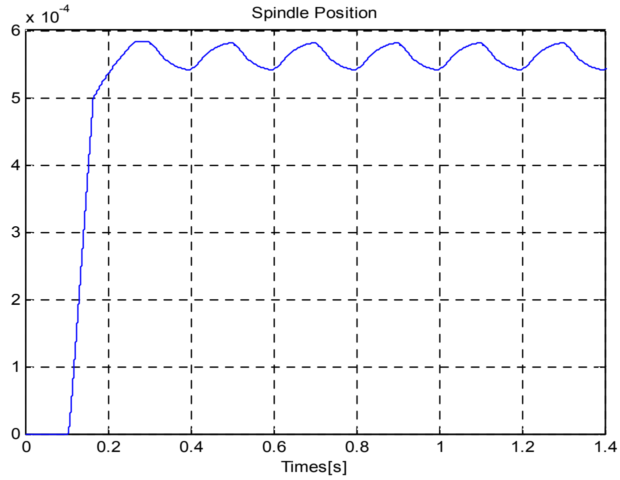

Fig. 8. Spindle position

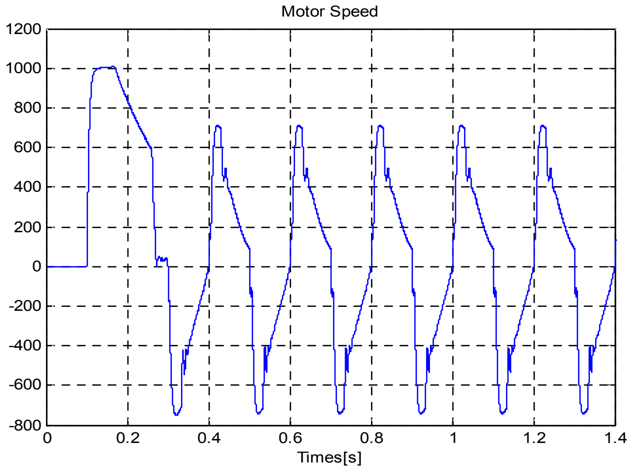

Fig. 9. Motor speed

mode, and can be explained from Fig. 4 and Fig. 8. Fig. 8 and Fig. 9 represent spindle position and motor speed during the simulation respectively. Fig. 8 shows that from 0 second to 0.1 second spindle position stays initial point, zero and then from 0.1 second spindle is moved by actuator. First, the position of spindle increases sharply for about 0.08 seconds then the EMB system starts clamping mode and it continues the mode until simulation is finished.

I. CONCLUSION AND FUTURE WORK

In this paper, we developed the complete model of EMB system and proved its validation by simulation using MATLAB SIMULINK. Then, we proposed the fuzzy logic control as an intelligent actuator controller logic and proved its verification by simulation, which shows that clamping force follows the command input accurately. Our next goal is to develop an intelligent actuator logic using adaptive fuzzy control for EMB system in noise and disturbance.

APPENDIX

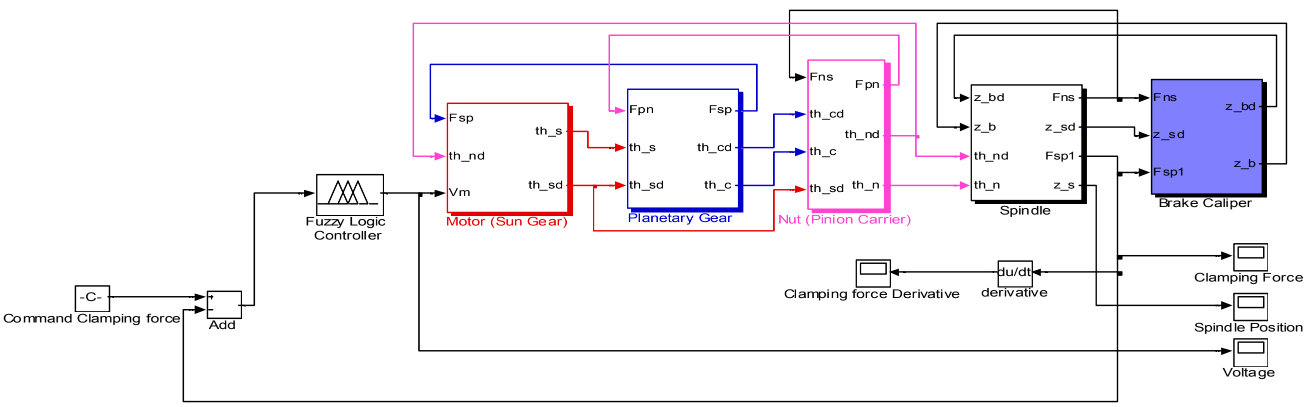

Fig. 10. SIMULINK Block for fuzzy logic control of EMB system

ISBN: 978-988-19251-2-1
ISSN: 2078-0958 (Print); ISSN: 2078-0966 (Online)

ACKNOWLEDGMENT

The authors gratefully acknowledge Hyundai motors and Mando corp. for their technical support of this research.

REFERENCES

[1] J. H. Kwank, B. Yao, A. Bajaj, "Analytical Model Development and Model Reduction for Electromechanical Brake System," American Society of Mechanical Engineers, Dynamic Systems and Control Division (Publication), 2004, pp. 297-306

[2] Jaeho Kwak, "Modeling and Control of an Electromechanical Brake (Brake-by-Wire) System," Purdue University, Doctoral dissertation, 2005

[3] Joogon Kim, Jongki Kim, "Cascade Control of Hybrid Brake System," Vol 2, 2008, pp. 757~760

[4] Wenzhe Lu, "Modeling and Control of Switched Reluctance Machines for Electro-Mechanical Brake System," Ohio State University, Doctoral dissertation, 2005

[5] Weidon Xiang, Paul C. Richardson, Chenming Zhao, and Syed Mohammad, "Automobile Brake-by-Wire Control System Design and Analysis," IEEE Transactions on Vehicular Technology, vol. 57, 2008, pp. 138-145

[6] Woohyun Hwang, Kwangjin Han, Kunsoo Huh, JooGon Kim, JongKi Kim, DongShin Kim, "Development of a Sensor Fault Diagnosis System for Electro-Mechanical Brake," KSAE, 2008, pp. 767-772

[7] Chih Feng Lee, Chris Manzie, Chris Line, "Explicit Nonlinear MPC of an Automotive Electromechanical Brake," the proceeding of IFAC, 2008

ISBN: 978-988-19251-2-1
ISSN: 2078-0958 (Print); ISSN: 2078-0966 (Online)